17th World Conference on Earthquake Engineering, 17WCEE
Sendai, Japan - September 13th to 18th 2020

Development of an Eddy Current Damper using a Ball Screw

S. Nakaminami[1], R. Masui[2] H. Kida[3], K. Imanishi[4]
Y. Kobashi[5], H. Nogami[6] Y. Takahashi[7], Y. Noguchi[8]

[1] *Aseismic Devices, CO., LTD., Technology Center, General manager, Dr. Eng., nakaminami@adc21.co.jp*
[2] *Nippon Steel Corporation, Osaka Steel Works, masui.cm6.ryohsuke@jp.nipponsteel.com*
[3] *Aseismic Devices, CO., LTD., Technology Planning DEP., General manager, Dr. Eng., hkida@adc21.co.jp*
[4] *Nippon Steel Corporation, Osaka Steel Works, General manager, Head of Department, imanishi.t3p.kenji@jp.nipponsteel.com*
[5] *Aseismic Devices, CO., LTD., Design Department, Chief Engineer, y-kobashi@adc21.co.jp*
[6] *Nippon Steel Corporation, Steel Research Laboratories, Chief Researcher, nogami.5ab.hiroshi@jp.nipponsteel.com*
[7] *Aseismic Devices, CO., LTD., Technology Planning DEP., takahashiy@adc21.co.jp*
[8] *Nippon Steel Corporation, Steel Research Laboratories, Chief Researcher, Dr. Eng., noguchi.yf5.yasutaka@jp.nipponsteel.com*

Abstract

Since earthquakes are a frequent occurrence in Japan, seismic control devices have long been widely used for civil structures. Seismic control devices are particularly effective for reducing the wind-induced or earthquake-induced response of high-rise buildings. Viscous dampers that are typical seismic control devices have temperature dependency and repeated load dependency for the viscous damping force. Therefore, the conventional devices are problematic in that the damping performance is reduced in long-period ground motions.

We propose a new eddy-current type damper (eRDT) to improve this issue. This device is converted from linear motion the ball screw to rotational motion of the pole ring by an amplifying mechanism. Permanent magnets are arranged on an outer surface of the pole ring and the braking ring made of steel, which faces the permanent magnets of the pole ring while maintaining a certain gap. When an earthquake occurs, a strong magnetic field is created and an eddy current is induced in the braking ring. As a result, the Lorentz force is generated and the reaction force acts in the inverse direction of the pole ring rotation. Therefore this device can absorb vibration energy of the building structure. In this paper, we describe the basic structure of the eRDT, and report the findings elicited from fundamental tests.

Keywords: Permanent Magnet, Eddy Current Damper, Lorentz Force, Amplification mechanism, Ball screw

1. Introduction

We have developed viscous-fluid type dampers using a ball screw (RDT) [1-3]. The RDT is a compact damper that generates a large viscous damping force because it has an amplification mechanism using a ball screw. However, the viscous damping force depends on both temperature and repeated load [4,5]. Therefore, when we design buildings, it was necessary to consider the reduction in the forces due to these effects. On the other hand, in the automotive field, a permanent magnetic retarder (PMR) [6] is known as auxiliary brakes for large-sized commercial vehicles. The PMR has low temperature dependency of eddy current brakes and requires no maintenance for decades. In previous papers, research on eddy-current dampers and implementation examples can be seen, but there are no development examples of 1,000 kN class dampers for civil structures [7-12]. Against this background, we have developed 1,000 kN class eddy-current type damper (eRDT) using a ball screw for buildings that applies the PMR technology to the RDT [13-16]. This paper describes the outline of the eRDT, the generating principle of the eddy-current damping of the eRDT. Also, we propose that the design formula of a total damping force of the eRDT considering both temperature and repeated load dependency based on results of the dynamic testing using a full-scale damper specimen.

2. Permanent magnetic retarder (PMR)

Fig.1 depicts a schematic representation of a permanent magnetic retarder (PMR). The PMR are used for auxiliary brakes such as trucks, buses and other medium- and large-sized commercial vehicles. The part consists of a rotor that is connected to the propeller shaft of a vehicle and that rotates and a stator having permanent magnets in it that is secured to the non-rotating section of the vehicle.

Fig.2 illustrates the main part forming the magnetic circuit of the PMR. When the rotor rotates in the magnetic field formed by the permanent magnets, eddy currents are generated on the rotor. The interaction between the currents and magnetic field generates Lorentz force in the direction opposite to the rotation direction. This force works as braking force that suppress the rotation of the propeller shaft. On and off of braking is switched by making the permanent magnets reciprocate in the circumferential direction using air cylinders. When the braking is on, the magnetic flux of the permanent magnets reaches the rotor through the pole pieces that are a ferromagnetic material, which generates braking force while the rotor is not in contact with the stator. When braking is off, a pole piece and the adjacent magnets from a closed circuit to prevent the magnetic flux from reaching the rotor. In this way, the magnets are moved by half of the arrangement interval of the pole pieces arranged in the circumferential direction to switch on and off of the braking.

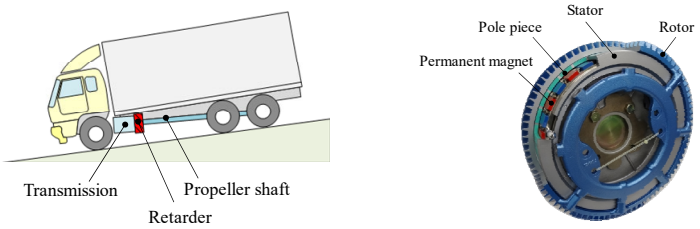

Fig. 1 – Schematic representation of a permanent magnetic retarder (PMR)

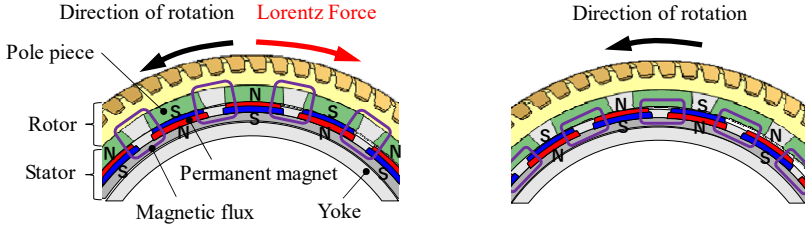

(a) Braking-on (b) Braking-off

Fig. 2 – Magnetic circuit of the PMR

3. Outline of an eddy-current type damper (eRDT)

Fig.3 depicts a schematic representation of an eddy-current type damper (eRDT). When applying the PMR technology to the RDT, we considered that the operating temperature, rotation speed, and durability were different from that for the vehicles, and the damper for buildings did not necessarily require the brakes to be turned on-off like a pole piece. In particular, we thought that permanent magnets were not likely to be affected by the performance decrement due to repeated load, which is a great advantage as a damper. The technology of the PMR was incorporated into the braking section. The shear resistive force due to the viscous-fluid, which is the damping force generation mechanism of the RDT [1-3] was replaced with the shear resistive force of the eddy-current. A ball screw was used for the amplification mechanism.

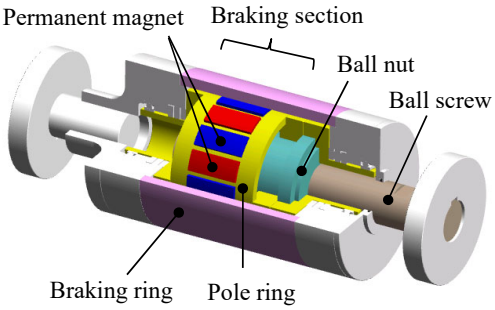

Fig. 3 – Schematic representation of an eddy-current type damper (eRDT)

The eRDT consists of a ball screw shaft, a ball nut, permanent magnets, a pole ring, and a braking ring. Neodymium magnets (Nd-Fe-B) were used as permanent magnets. A plurality of the permanent magnets were attached along the outer peripheral surface of the pole ring. The poles of the permanent magnet are magnetized in the radial direction. Adjacent magnetic poles are located on different poles. The material of the pole ring is a ferromagnetic material. The pole ring has a role of a yoke that makes it difficult for the magnetic flux from the permanent magnet to leak outside. The pole ring is structured to rotate in accordance with the rotation of the ball nut. Since an eddy current is generated on the inner peripheral surface of the braking ring, it is made of a material having magnetism and conductivity. The inner peripheral surface of the braking ring and the permanent magnet face each other with a gap.

4. Generating principle of an eddy-current force of the eRDT

Fig. 4 depicts the generating mechanism of an eddy-current force of the eRDT. When the ball screw shaft moves in the axial direction occurred to shaking such as earthquakes, the ball nut and the pole ring rotate, so that permanent magnets attached to the pole ring rotates. Therefore, the relative velocity is generated between the braking ring and the pole ring, and a fluctuating magnetic field is generated on the surface of the braking ring. Eddy currents are generated on the braking ring surface by the action of the fluctuating magnetic field, and a Lorentz force is generated by an interaction between the eddy current and the magnetic force. The resistive force is generated in a direction opposite to the ratation of the pole ring. This force become the main damping force of the eRDT.

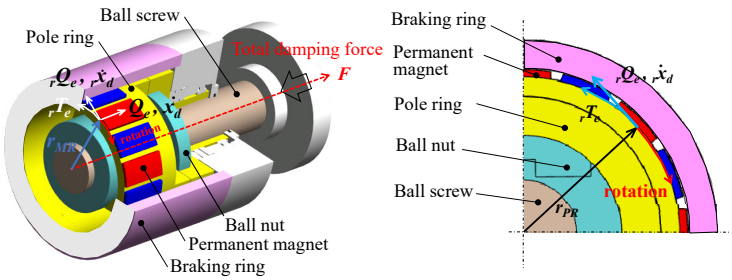

Fig. 4 – Generating mechanism of an eddy current force the eRDT

5. Specimen Outline

Table 1 lists the specifications of the eRDT specimen, Fig. 5 shows explanation of item and notion of the eRDT. The specimen was designed to the maximum total forces of 1,000 kN at maximum velocity of 15cm/s for seismic control of buildings. The length is 1,100 mm, the outer diameter is 365 mm, the stroke is ± 100 mm, and the weight is 530 kg. The braking section was designed so that the maximum braking torques would be 2.3 kN-m when the rotation speed of the ball nut was 450 rpm.

Table 1 – Specifications of specimen

Item		Notion	Unit	value
Length		L	mm	1,100
Stroke		S_t	mm	±100
Weight		W	mm	530
Amplification section	Diameter of ball screw	D_B	mm	100
	Lead of ball screw	L_d	mm	20
Braking section	Diameter of braking ring	D_{BR}	mm	365
	Diameter of pole ring	D_{PR}	mm	295
	Amplification factor	S_{PR}	mm	46
	Inertance	m_d	ton	150

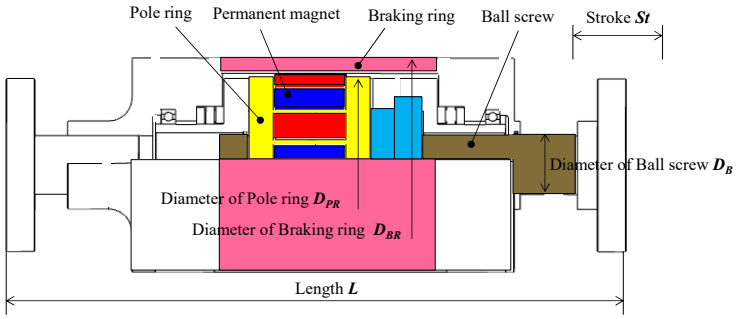

Fig. 5 – Explanation of Item and Notion of the eRDT

6. Experimental Setup

Fig. 6 and 7 shows the schematics and photographs of the experimental setup, respectively. The specimen was installed via a clevis joint on a portal frame equipped with a 3,000 kN dynamic actuator (Maximum forces ± 3,000 kN, Maximum velocity ± 30 cm/s, Stroke ± 100 mm).

The measured points were the load of the actuator, displacement of the actuator, the relative displacement of the damper, the displacement of the clevis joint, the temperatures around the permanent magnets, and an ambient temperature.

The input waveform for confirming the basic performance of the eRDT was 5 cycle of sine wave with taper. The input frequency was 0.1-1.0 Hz, the input amplitude was ± 2-60 mm, and the maximum velocity was 0.13-18.8 cm/s. In addition, 1cycle of ramp wave was input to confirm the friction resistive force of the eRDT at low velocity (Amplitude ± 80 mm, Velocity ± 0.1 cm/s).

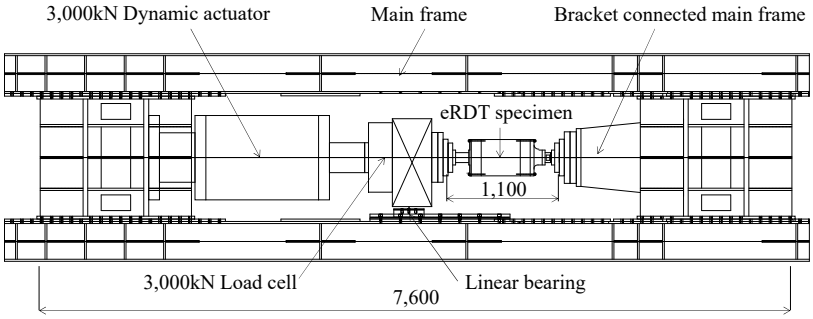

Fig. 6 –Experimental Setup

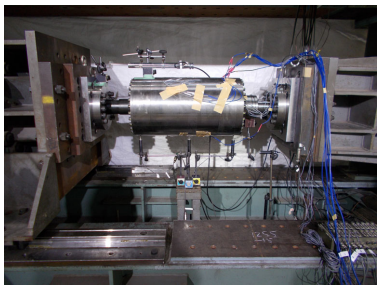

Fig. 7 – Photograph of experimental setup

7. Experimental Results

7.1 Hysteresis loops

Fig. 8 and 9 depicts the hysteresis loops of ramp wave and sin wave for frequency of 0.1 Hz, 0.2 Hz, 0.3 Hz, 0.5 Hz, respectively. The test starting temperature was 20 ℃. As shown in Fig. 8, a rectangular hysteresis characteristic can be seen at low velocity range. Since the resistive force generated by the eddy current has almost no effect at the low velocity range, this hysteresis characteristic is considered to be caused by mechanical friction. Also, it can be seen that as the amplitude increases, the history loops show a history characteristic as if an ellipse were added to a rectangle. This hysteresis characteristic is considered to be the effect of the resistive force due to eddy currents. Furthermore, it can be seen that as the frequency increases, the hysteresis characteristic tilts to the right. This is considered to be the effect of the inertial forces.

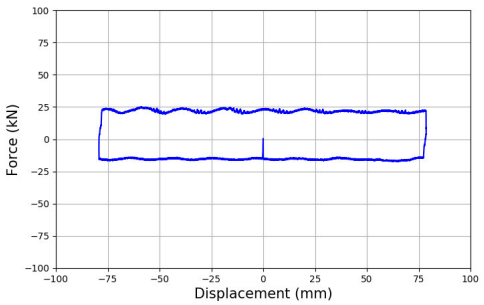

Fig. 8 – Hysteresis loops of ramp wave

7.2 Velocity and Frequency dependency of the total damping force

Fig. 10 (a) depicts the total damping force-velocity relationship of the first cycle in the axial direction of the ball screw. As shown in Fig. 10 (a), it can be seen that the total damping force shows a large increase at the low velocity, and shows a non-linear characteristic as the velocity increases. There is almost no change in the

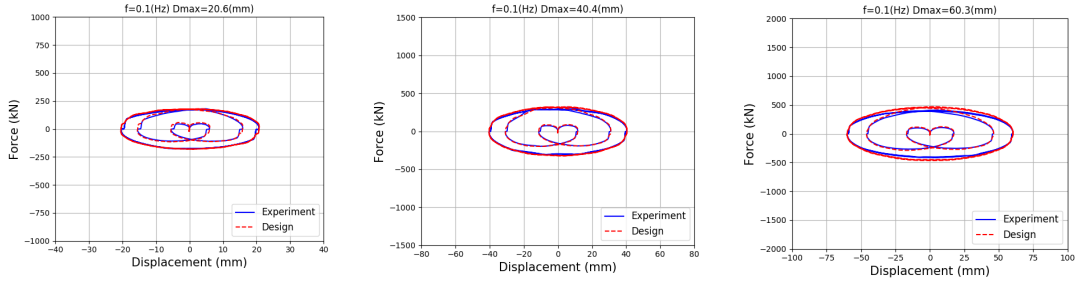

(a) 0.1 Hz

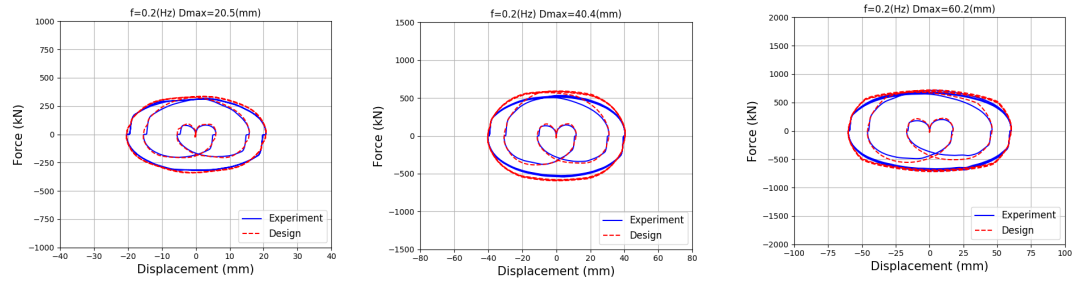

(b) 0.2 Hz

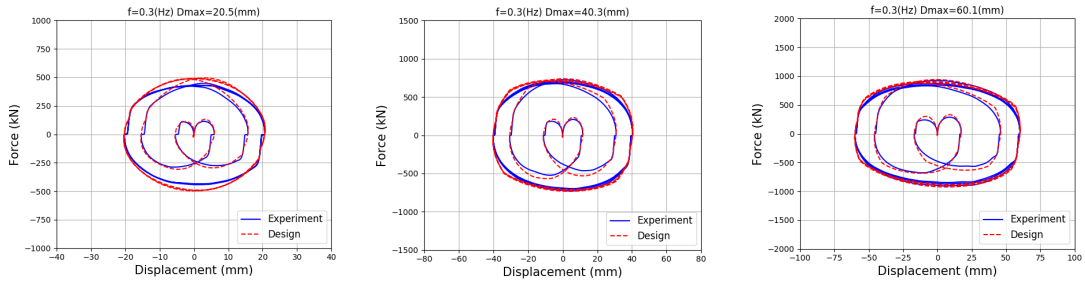

(c) 0.3 Hz

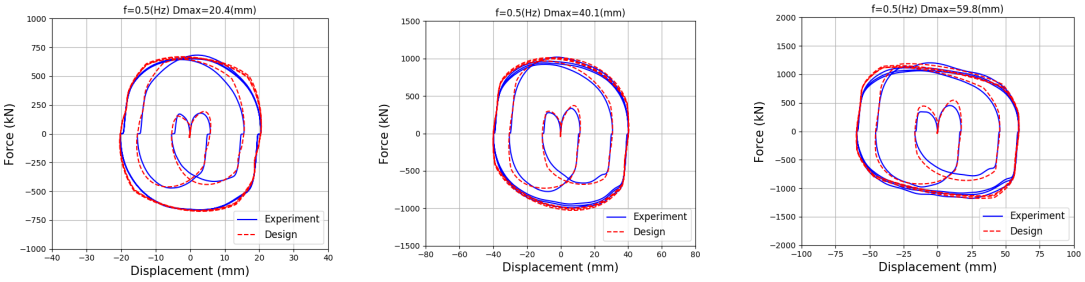

(d) 0.5Hz

Fig. 9 – Hysteresis loops of sin wave

total damping force-velocity relationship due to the difference in frequency, and it can be said that there is no frequency dependency of the total damping force. Fig. 10 (b) depicts the eddy current force-velocity relationship of the first cycle in the axial direction of the ball screw. The conversion from the total damping force F to the eddy current force Q_e was calculated by Eq. (1).

$$Q_e = \left(\frac{F}{\lambda}\right) - Q_i - Q_f \tag{1}$$

Where, the convention efficiency of a ball screw λ = 1.40, the frictional forces Q_f = 20 kN, inertia mass for calculating inertial forces Q_i = 150ton. As shown in Fig. 10 (b), the ratio of the eddy current force to the total damping force is about 70%.

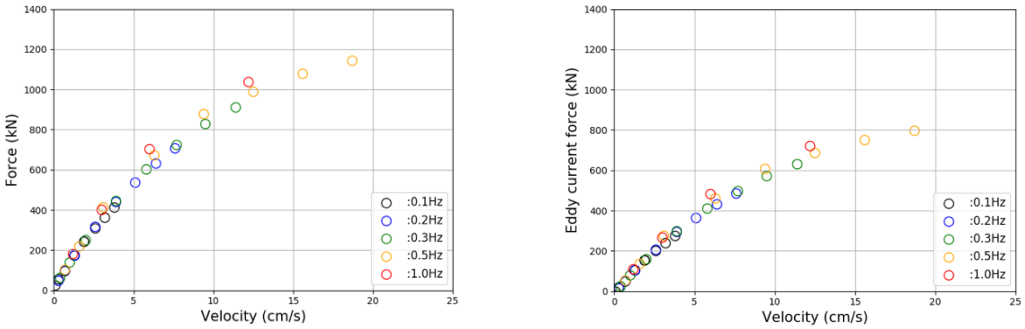

(a) Total damping force (b) Eddy current force

Fig. 10 – Velocity and frequency dependency

Fig. 11 depicts torques due to the eddy current force-rotational speed relationship of the first cycle. The conversion from the eddy current force (kN) to the torque (kN-m) was calculated by Eq. (2). The conversion from the velocity (cm/s) of the axial direction to the rotational speed (rpm) was calculated by Eq. (3). As shown in Fig. 11, it was confirmed that the setting of the eddy current force was as designed.

$$ {}_rT_e = Q_e \times \frac{L_d}{2\pi} \qquad (2) \qquad N = \dot{x}_d \times \frac{60}{L_d} \qquad (3) $$

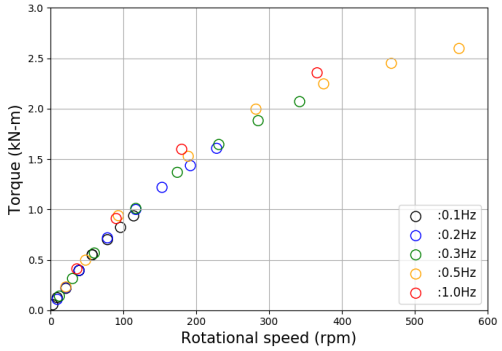

Fig. 11 – Torque-rotational speed relationship

7.3 Temperature dependency of the eddy current force

Fig. 12 and 13 depicts the eddy current force-velocity relationship of the first cycle in the range of from -5 to 50 ℃, and the measurement point of the temperatures around the permanent magnets, respectively. In confirming the temperature dependency of the eddy current force, it was difficult to testing under a wide range of ambient temperature. Therefore, the test starting temperature at measurement point ② was regarded as the ambient temperature and evaluated. The temperature difference between measurement point ② and measurement point ① was within ± 1 ℃. The data were grouped into a range of ±2.5 ℃ for each of -5, 0, 10, 15, 25, 30, 40, 45, and 50 ℃. The reference temperature for design was 20 ℃.

As shown in Fig. 12, there is almost no temperature dependency at the high temperature side with respect to the design temperature of 20 ℃, but the temperature dependency can be confirmed at the low temperature side. The scatter of the eddy current force was -5.7% to 26.3% compared to that at the design temperature of

20 ° C. Since the change in magnetic flux density due to the temperature of a general neo-simultaneous magnet is -0.12 % per ℃, the low-temperature side scattering is considered to be a mechanical factor other than permanent magnets, such as an increase in resistance force due to the temperature dependency of grease used in ball screws and bearings. The problem of the decrease in damping force caused by the temperature rise due to the repeated load is a problem on the high temperature side, and Fig. 12 shows that the eRDT can improve these problems.

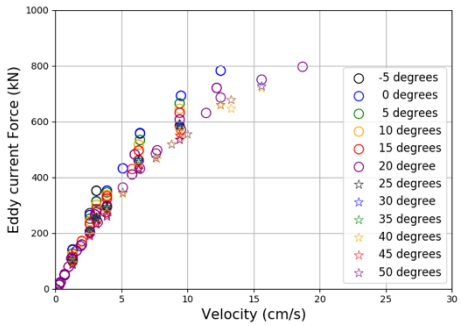

Fig. 12 – Temperature dependency of eddy current force

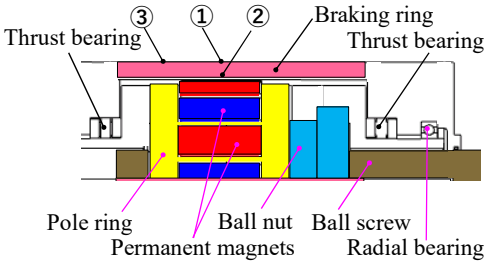

Fig. 13 – Measurement points of temperatures

7.4 Repeated load dependency of the total damping force

Fig. 14 depicts temperature rise-cumulative energy of the total damping force relationship. As shown in Fig. 14, It was found that the temperature rise and the cumulative energy have approximately linear relationship, and this relationship is expressed by Eq. (4).

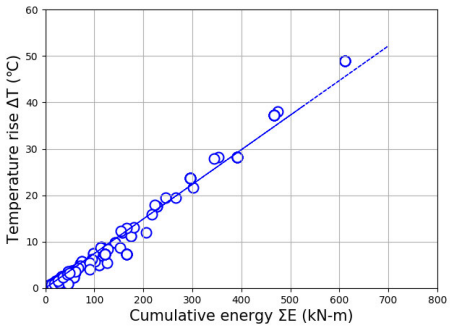

Fig. 14 – Temperature rise-energy relationship

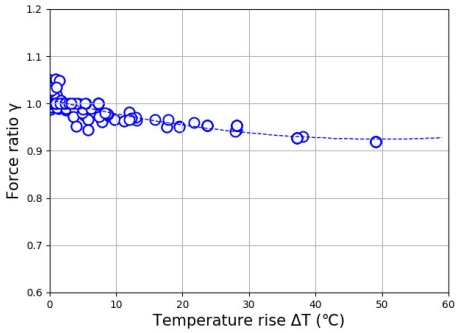

Fig. 15 – Force ratio-temperature rise relationship

$$\Delta T = 0.0745 \cdot \Sigma E \tag{4}$$

Where ΔT is the temperature rise of at measurement point ②, ΣE is the cumulative energy of the total damping force. Fig. 15 depicts the force reduction ratio of each cycle against the force of 1st cycle-temperature rise (Force ratio γ) relationship at measurement point ②. γ is expressed by Eq. (5).

$$\gamma = 0.0000336 \cdot \Delta T^2 - 0.00335\Delta T + 1.0084 \tag{5}$$

Where γ is the force reduction ratio of each cycle against the force of 1st cycle. As shown in Fig. 15, γ was approximately 0.93 at 50 ° C., and it was confirmed that the eRDT had high performance with respect to the repeated load dependency.

As described above, the temperature rise due to the cumulative energy can be estimated by the Eq. (4), and the force reduction ratio of each cycle against the force of 1st cycle due to the temperature rise can be evaluated by Eq. (5). Here, the design limit temperature of the permanent magnets is approximately 120 ℃.

8. Design formula for total damping force of the eRDT

8.1 Composition of total damping force

Fig. 16 and 17 illustrates the composition of total damping force of the eRDT, and the analysis model of the eRDT, respectively. K_b in Fig. 16 indicates the axial rigidity of the damper. The total damping force of the eRDT is expressed as the combined force when the eddy current force Q_e, inertia force Q_i, and frictional force Q_f generated in the braking section work on the convention efficiency of the ball screw [2].

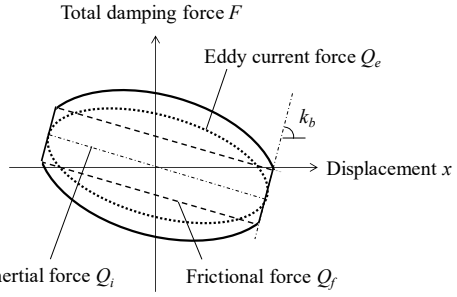

Fig. 16 – Composition of total damping force

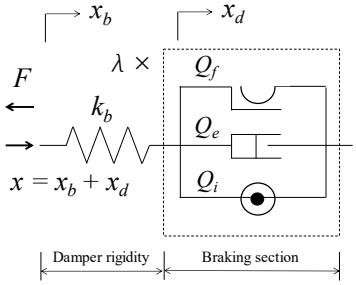

Fig. 17 – Analytical model of the eRDT

Thus, the total damping force F of the eRDT is derived from the following equation:

$$F = \lambda(Q_e + Q_i + Q_f) \tag{6}$$

Where λ is the convention efficiency of a ball screw, is the following equation:

$$\lambda = \frac{1}{1 - \frac{\mu_B\left(\frac{1}{tan\theta} + tan\theta\right)}{1 + \mu_B tan\theta} - \mu_{SB}\alpha_{SB}} \tag{7}$$

Where μ_B and $tan\theta$ are the friction coefficient of the ball screw and lead angle of the ball screw, μ_{SB} is the friction coefficient of the thrust bearing, and α_{SB} is the amplification factor at the center diameter of the thrust bearing ($=2\pi r_{SB} / L_d$). L_d is the lead of the ball screw. The eddy current force Q_e generated in the axial direction of the ball screw is expressed by Eq. (8).

$$Q_e = \left(\frac{2\pi r_{PR}}{L_d}\right) {}_rQ_e = \alpha_{PR}\left(\frac{{}_rT_e}{r_{PR}}\right) \tag{8}$$

Q_e is expressed by multiplying the amplification factor α_{PR} ($= 2\pi r_{PR} / L_d$) at the outer radius of the pole ring by the circumferential eddy current force ${}_rQ_e$ generated on the inner surface of the pole ring. ${}_rQ_e$ is equal to the torque force ${}_rT_e$ divided by the pole ring outer radius as shown in Eq. (9).

$$ {}_r\dot{x}_d = \dot{x}_d\left(\frac{2\pi r_{PR}}{L_d}\right) = \dot{x}_d\alpha_{PR} \tag{9}$$

The rotational velocity ${}_r\dot{x}_d$ of the pole ling is expressed values obtained by multiplying the axial velocity $\dot{x}_d$ of the ball screw by α_{PR}. The relationship between Eq. (8) and (9) shows that the eddy current force is a force that depends on the rotation speed. Therefore, the eddy current force can be represented as a dash-pot model that generates damping forces depending on the velocity as shown in Fig. 6.

The inertial force Q_i generated in the axial direction of the ball screw is expressed by Eq. (10).

$$Q_i = J\left(\frac{2\pi}{L_d}\right)^2 \ddot{x}_d = m_d \ddot{x}_d \tag{10}$$

Where J and $\ddot{x}_d$ are the moment of inertia of the ball-nut and pole-ring about the ball screw axis, the linear relative acceleration. Q_i is expressed by multiplying an apparent mass m_d by $\ddot{x}_d$. m_d is expressed by multiplying the moment of inertia by ampilification factor $(2\pi/L_d)^2$.

8.2 Evaluation of design formula of the eddy current force

In this section, we propose the design formula of the eddy current force considering both the temperature dependency and repeated load dependency obtained in the sections 7.3 and 7.4. First, the data of relationship between the eddy current force and velocity at temperatures from -5 to 50 ° C was by tri-linear model as shown in Fig. 18 (a). Next, the evaluation formula of the eddy current force considering the temperature dependency was created from each coefficient of the tri-linear model at each temperature. This evaluation formula is expressed by Eq. (11). Fig. 18 (b) shows design curves from −5 to 50 ° C obtained from Eq. (11). Drawing of the design curves shown Fig. 18 (b) in was performed up to the velocity confirmed in the experiment at each temperature. The scatter between the experimental values shown in Fig. 13 and the design curves was -13.2% to + 14.3%.

Here, the total damping force F considering the temperature dependency is obtained by substituting λ = 1.4, Q_e equals Eq. (11), Q_f = 20 kN, and Q_i equals Eq. (10) into Eq. (6).

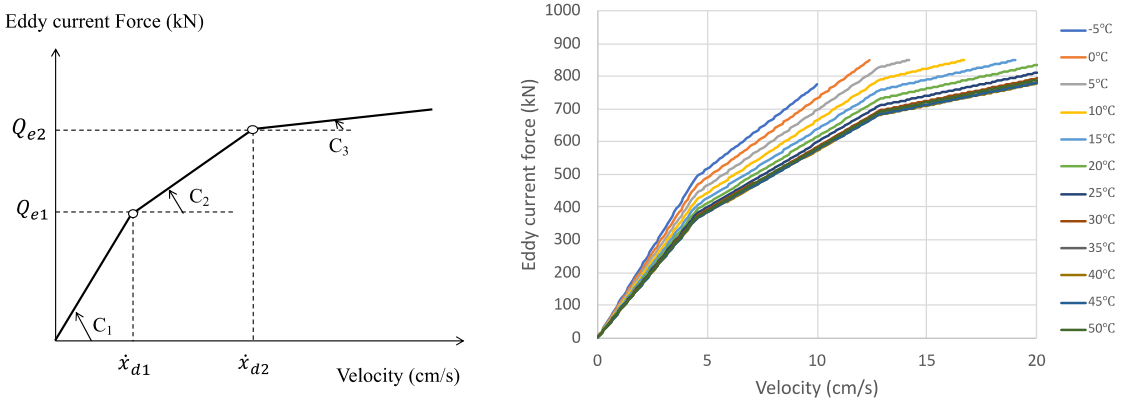

(a)Tri-linear model (b) Design curves of from -5 to 50 ℃

Fig. 18 – Analytical model of the velocity-the eddy current force relationship

$$\begin{cases} Q_e = C_1 \cdot \dot{x}_d & (\dot{x}_d \le \dot{x}_{d1}) \\ Q_e = C_2(\dot{x}_d - \dot{x}_{d1}) + Q_{e1} & (\dot{x}_{d1} < \dot{x}_d < \dot{x}_{d2}) \\ Q_e = C_3(\dot{x}_d - \dot{x}_{d2}) + Q_{e2} & (\dot{x}_{d2} \le \dot{x}_d) \end{cases} \tag{11}$$

Where

Q_e : Eddy current force (kN)

$\dot{x}_d$: Velocity (cm/s)

C_1 : 1st damping coefficient $C_1 = 0.013T^2 - 1.11T + 103$

C_2 : 2nd damping coefficient $C_2 = 29.1\beta$

C_3 : 3rd damping coefficient $C_3 = 14.4\beta$

$\dot{x}_{d1}$: 1st yield velocity (cm/s) $\dot{x}_{d1} = 206.7\beta/(C_1 - C_2)$

$\dot{x}_{d2}$: 2nd yield velocity (cm/s) $\dot{x}_{d2} = 12.9$

Q_{e1} : 1st yield force (kN) $Q_{e1} = C_1 \cdot \dot{x}_{d1}$

Q_{e2} : 2nd yield force (kN) $Q_{e2} = C_3 \cdot \dot{x}_{d2} + 545.2\beta$

β : Temperature factor $\beta = 0.000155T^2 - 0.0127T + 1.193$

T : Ambient temperature (℃)

Also, the total damping force F considering the repeated dependency in addition to the temperature dependency can be obtained by multiplying Eq. (6) by γ shown in Eq. (5), and is the following equation:

$$F = \gamma \cdot \lambda\left(Q_e + Q_i + Q_f\right) \tag{12}$$

Fig. 9 shows comparisons between experimental values and design curves in sine wave. As shown in Fig. 9, the two values are almost identical, it was confirmed that validity of the evaluation formula of the total damping force of the eRDT.

9. Conclusions

This paper proposed a new eddy-current type damper (eRDT) using a ball screw for the seismic control of buildings that applies the PMR technology to the RDT. Dynamic testing was conducted using a full-scale damper specimen. The experimental results using sinusoidal excitation showed that the temperature dependency on the high-temperature side was very small, and the reduction in damping force due to repeated load was small. It was showed that the evaluation formula of the eddy current force Q_e considering both the temperature dependency and repeated load dependency can be modeling in tri-liear model considering the velocity dependency. It was confirmed that the total damping force could be evaluated by replacing this Q_e with the viscous damping force Q_v of the conventional RDT design formula.

The authors would like to futher investigate the performance reduction due to large amplitudes and long-term repeated loading and the eddy current forces by low temperature testing at high velocity range, and to improve the accuracy of the evaluation formula proposed in this paper.

10. References

[1] Arima F., Inoue Y., Baba K., Kuroda H., Aragaki T., (1998): Development of the seismic damper with amplified mechanism, Part1: Damping properties of the RD-Tube applied to ball screw, *Annual meeting of Architectural Institute of Japan,* B-2, 825-826 (in Japanese).

[2] Kuroda H., Arima F., Baba K., Inoue Y., (2000): Principles and characteristics of viscous damping devices (GYRO-DAMPER), The damping forces which are highly amplified by converting the axial movement to rotary

one. *Proceedings of the 12th World Conference on Earthquake Engineering,* Auckland, New Zealand, Paper ID 0588.

[3] Saito K., Yogo K., Sugimura Y., Nakaminami S., Park K., (2004): Application of rotary inertia to displacement reduction for vibration control system. *Proceedings of the 13th World Conference on Earthquake Engineering,* Vancouver, B.C., Canada, Paper ID 1764.

[4] Nakaminami S., Kuroda H., Arima F., Suzuki R., Inoue Y., Baba K., (2000): Development of the seismic damper with amplified mechanism, Part6: Evaluation method of viscous damping force by rheometer, *Annual meeting of Architectural Institute of Japan,* B-2, 873-874 (in Japanese).

[5] Nakaminami S., Furuhashi T., Mitsusaka K., Suzuki T., Saito K., Nakazawa A., (2003): Performance evaluation of the seismic damper with amplified mechanism in high velocity range, Part3: Viscous damping force in high shear rate range, *Annual meeting of Architectural Institute of Japan,* B-2, 763-764 (in Japanese).

[6] Nogami H., Tasaka M., Kadokawa S., Fujita T., Imanishi K., Noguchi Y., Fujimoto H., Miyasaka M., (2019): Development of a new high-efficiency, lightweight model of permanent magnetic retarder, *NIPPON STEEL TECHNICAL REPORT No.122 NOVEMBER 2019*, 137-144.

[7] Sodano H.A., Bae J.S., (2004): Eddy current damping in structures, *Shock and Vibration Digest 36(6)*, 469-478.

[8] Kwang D.G., Bae J.S., and Hwang J.H., (2007): Experimental study for dynamic characteristics of an eddy current shock absorber, *Journal of the Korean Society Aeronautical and Space Sciences 35(12)*, 1089-1094.

[9] Cheah S.K. and Sodano H.A., (2008): Novel eddy current damping mechanism for passive magnetic bearings, *Journal of Vibration and Control 14(11)*, 1749-1766.

[10] Bae J.S., Hwang J.H., Park J.S., Kwang D.G., (2009): Modeling and experiments on eddy current damping caused by a permanent magnet in a conductive tube, *Journal of Mechanical Science and Technology 23(11)*, 3024-3035.

[11] Zuo L., Nayfeh S., Chen X.M., (2011): Design and analysis a new type of electromagnetic damper with increased energy density, *Journal of Vibration and Acoustics 133(4)*, 041006.

[12] Pan Q., He T., Xiao D., Liu X., (2016): Design and damping analysis of a new eddy current damper for aerospace applications, *Latin American Journal Solids and Strictures 13*, 1997-2011.

[13] Nakaminami S., Masui R., Kida H., Imanishi K., Kobashi Y., Nogami H., Takahashi Y., Noguchi Y., (2019): Development of an eddy current damper using a ball screw, Part1: Outline of the damper, *Annual meeting of Architectural Institute of Japan,* B-2, 785-786 (in Japanese).

[14] Masui R., Nakaminami S., Imanishi K., Kida H., Nogami H., Kobashi Y., Noguchi Y., Takahashi Y., (2019): Development of an eddy current damper using a ball screw, Part2: Evaluation of an eddy current force, *Annual meeting of Architectural Institute of Japan,* B-2, 787-788 (in Japanese).

[15] Kobashi Y., Masui R., Nakaminami S., Imanishi K., Kida H., Nogami H., Noguchi Y., Takahashi Y., (2019): Development of an eddy current damper using a ball screw, Part3: Evaluation of temperature and cyclic dependence, *Annual meeting of Architectural Institute of Japan,* B-2, 789-790 (in Japanese).

[16] Masui R., Imanishi K., Nogami H., Noguchi Y., Nakaminami S., Kida H., Kobashi Y., Takahashi Y., (2019): Development of an eddy current damper, *Annual meeting of Mechanical Institute of Japan, No.19-1*, J10312 (in Japanese).

